Accepted Version

Cite as: H. Sharma, N. Zerbe, C. Böger, S. Wienert, O. Hellwich and P. Hufnagl, "A Comparative Study of Cell Nuclei Attributed Relational Graphs for Knowledge Description and Categorization in Histopathological Gastric Cancer Whole Slide Images," *2017 IEEE 30th International Symposium on Computer-Based Medical Systems (CBMS)*, Thessaloniki, 2017, pp. 61-66, doi: 10.1109/CBMS.2017.25.

A comparative study of cell nuclei attributed relational graphs for knowledge description and categorization in histopathological gastric cancer whole slide images

Harshita Sharma[1], Norman Zerbe[2], Christine Böger[3], Stephan Wienert[2], Olaf Hellwich[1] and Peter Hufnagl[2]
[1] *Computer Vision and Remote Sensing, Technical University Berlin, Berlin, Germany*
[2]*Department of Digital Pathology and IT, Institute of Pathology, Charité University Hospital, Berlin, Germany*
[3]*Department of Pathology, Christian-Albrechts University, Kiel, Germany*

***Abstract*—In this paper, cell nuclei attributed relational graphs are extensively studied and comparatively analyzed for effective knowledge description and classification in H&E stained whole slide images of gastric cancer. This includes design and implementation of multiple graph variations with diverse tissue component characteristics and architectural properties to obtain enhanced image representations, followed by hierarchical ensemble learning and classification. A detailed comparative analysis of the proposed graph-based methods, also with the established low-level, object-level and high-level image descriptions is performed, that further leads to a hybrid approach combining salient visual information. Quantitative evaluation of investigated methods suggests the suitability of particular graph variants for automatic classification using H&E stained histopathological gastric cancer whole slide images based on HER2 immunohistochemistry.**

***Keywords*-Cell nuclei attributed relational graphs, H&E stain, gastric cancer, knowledge description, automatic classification, biomedical image analysis, digital histopathology.**

I. Introduction

Graph is a powerful structure widely studied for image analysis in digital histopathology [1], as it can suitably describe significant visual characteristics of histological images by incorporating the knowledge of spatial arrangements, structural properties and neighborhood relationships between tissue components. The cell nuclei attributed relational graph (*cell nuclei ARG*) is a novel image representation and feature extraction method, analyzed for automatic classification in haematoxylin and eosin (H&E) stained whole slide images (WSI) of gastric carcinoma, based on HER2 immunohistochemistry (IHC) [2]. In principle, the cell nuclei ARG for a magnified tissue image is constructed by computing and assigning numerical attributes to its vertices (cell nuclei) and edges (links with neighbors), to describe their individual component characteristics, spatial interactions and underlying tissue architecture. The basic cell nuclei ARG method has revealed favorable initial outcome compared to most of the frequently applied histopathological feature extraction approaches, namely, low-level (pixel-based) features including texture, color and intensity, and high-level (architectural) features including Voronoi diagrams and Delaunay triangulation, followed by AdaBoost classification [2]. Therefore, the capabilities of cell nuclei ARG require to be further investigated for potential enhancements. This paper contributes towards an extension of the preliminary algorithm by systematic formulation and empirical analysis of multiple variations in the cell nuclei ARG. The proposed methods are quantitatively analyzed to examine their relative discriminative power, along with comparison with state-of-the-art feature extraction in digital histopathology [3], namely, pixel-based, object-level and architectural methods, using hierarchical random forests ensemble learning and classification. The experimental results establish the ability of proposed graph-based methods to obtain meaningful knowledge description and automatic categorization in H&E stained gastric cancer WSI.

In literature, a graph-based method called *cell graph* [4], [5] is explored primarily for H&E stained brain cancer and breast tissue images, and described more suitable than proximity graphs [6] especially due to less geometrical constraints for cancer tissue modeling. In our work, the proposed cell nuclei ARG and its variants have also been conceptualized with fewer linking constraints. However, the cell nuclei ARG is constructed at a higher magnification by computing visual characteristics of individual cell nuclei, their neighborhoods and relational information between neighbors. The edge linking rules and global graph features are also distinct from cell graphs. Attributed relational graphs have been recently explored for image analysis tasks in digital histopathology. For instance, attributed relational regional adjacency graphs have shown promising results for content-based image retrieval in breast cancer biopsies [7]. Attribute relational graphs are also applied for segmenting cell nuclei using a model-based approach in fluorescence microscopy images of hepatocellular carcinoma [8]. Attributed minimum spanning trees have been explored [9] for representation in Feulgen stained soft tissue tumors. Related to this work, a multiresolution approach is developed [10] to enhance cell nuclei segmentation for an accurate graph construction, and includes a supervised cell nuclei classification utilized in graph design variations in gastric cancer WSI.

The paper is organized as follows. Section II describes the developed methods and Section III discusses the experimental results. Section IV presents the conclusion and future research directions of this work.

II. Methods

Figure 1 illustrates the schematic overview of the proposed method, explained in detail in the following sections.

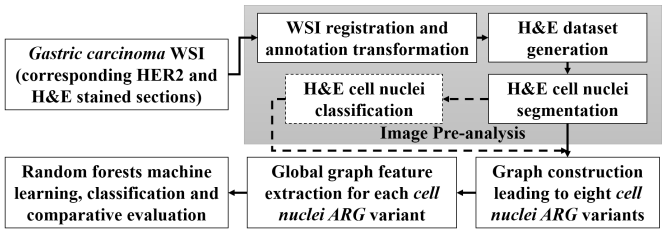

Figure 1: Schematic overview

A. Gastric Carcinoma WSI Datasets

HER2 immunohistochemical staining has been recently introduced as a biomarker for gastric cancer, along with a *10% cut-off rule* [11] to study inter-and intra-observer variability among pathologists. H&E stain is routinely used due to clear staining of cell nuclei, easy application and lower preparation costs [12], thus, it has been preferably analyzed in this work. The main objective is to implement advanced methods for appropriate knowledge description and categorization in the H&E stain, which is more difficult to visually discern compared to the HER2 IHC stain.

The experimental data consists of 11 whole slide images in HER2 and H&E stain, acquired from surgical sections of distinct patients of *gastric adenocarcinoma* [11], [13]. The HER2 IHC stained WSI contain annotations by ten pathologists for HER2 positive tumor (HER2+) and HER2 negative tumor (HER2-) regions, where HER2+ tumor areas follow the 10% cut-off rule and represent higher malignancy, and HER2- tumor areas are morphologically identified as tumor and denote lower malignancy. Corresponding H&E stained sections are scanned by *3D Histech Panoramic 250* scanner with resolution 0.22 μm/pixel (at 40$\times$ objective magnification) with quadratic pixels.

B. Image Pre-analysis

Image pre-analysis includes a semi-automatic registration followed by a transformation of pathologists' annotation originally created in HER2 WSI to the H&E WSI [2]. The H&E WSI are tessellated at 40$\times$ objective magnification, with each image tile of size 1024 $\times$ 1024 pixels, to provide large fields of view containing rich context information. Non-overlapping image tiles are selected from areas inside polygon annotations of HER2+ tumor and HER2- tumor considering regions of agreement of most pathologists. Non-tumor category comprises of regions lying outside both types of polygon annotations. This is followed by cell nuclei segmentation [14] and optional cell nuclei classification [10] (applied to a subset of the cell nuclei ARG variants). Cell nuclei classification has been modified in class definitions of cell nuclei segments as one of the seven categories, namely, epithelial cells, leukocytes, fibrocytes, conglomerates, fragments, other cells and artefacs, along with random forests machine learning, leading to an overall superior multi-class accuracy (*ca.* 65%), with the diagnostically relevant cell nuclei classes showing relatively high prediction rates.

C. Cell Nuclei ARG Construction

An attributed relational graph $G(V, E, A, B)$ consists of vertices V, edges E and their associated attributes A and B respectively [7]. The attributes of a vertex $v_i \in V$ are represented by vector $\mathbf{a_i} = [a_i^{(p)}], (p = 1, 2, 3, ..., P, \mathbf{a_i} \in A)$, and attributes of edge $e_{ij} \in E$ between $v_i, v_j \in V$ by vector $\mathbf{b_{ij}} = [b_{ij}^{(q)}], (q = 1, 2, 3, ..., Q, \mathbf{b_{ij}} \in B)$. The *cell nuclei ARG* is constructed by considering the cell nuclei segments as graph vertices [2]. Vertex v_j is included in the neighborhood $N_{i,j}$ of vertex v_i if and only if,

$$d_e(i, j) \leq r \tag{1}$$

where $d_e(i, j)$ denotes the Euclidean distance between the centroids of v_i and v_j, and r is called *maximum spanning edge length*. Attribute vectors are assigned to each vertex and edge [2], where each $\mathbf{a_i}$ includes the morphological, contour intensity and neighborhood-based properties of the corresponding cell nucleus, and each $\mathbf{b_{ij}}$ represents the Euclidean lengths, orientations and absolute vertex attribute differences between neighboring vertices.

D. Proposed Variants of the Cell Nuclei ARG

The two design variables are linking rule to determine r and construction method based on vertex information.

1) Linking rule to determine r: The two linking rules to determine maximum spanning edge length r are as follows.
Fixed $\mathbf{r}(r_F)$: Here, r is empirically predetermined for all the images irrespective of malignancy type by visual inspection of graph structures to represent unique neighborhood and architectural characteristics of the three malignancy groups. It is visually and quantitatively observed that an adequately estimated value of r_F can lead to powerful cell nuclei ARG descriptions of the gastric cancer tissue.
Adaptive $\mathbf{r}(r_A)$: A dynamic value of r is computed for each image region before graph construction, depending on its cell nuclei density. An imaginary regular grid consisting of equal sized rectangular grid cells is considered, assuming that each grid cell consists of a cell nuclei centroid at its center. r is the maximum distance between the given cell nuclei centroid and its 8-neighbors. Let the length of the image tile be l, breadth b, number of grid cells in each row N_l and in each column N_b (depicted in Figure 2).

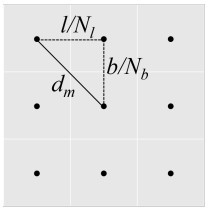

Figure 2: Regular grid assumption to determine r_A

The maximum distance d_m of a grid cell center with its 8-neighbors is given by

$$d_m = \sqrt{\left(\frac{l}{N_l}\right)^2 + \left(\frac{b}{N_b}\right)^2} \tag{2}$$

For a square image tile, $l = b$ and $N_l = N_b = N$, therefore,

$$d_m = \sqrt{\frac{2l^2}{N^2}} = \frac{\sqrt{2}l}{\sqrt{N_v}} \tag{3}$$

where, N^2 is the total number of grid cells. Also, according to the assumption, each grid cell consists of a cell nuclei centroid, so N^2 is the total number of vertices N_v in the cell nuclei ARG. To obtain the value of r_A for an image tile, d_m is rounded off to the nearest higher integer. The main advantage of this approach is the elimination of the prerequisite of empirically fixing r as it is automatically calculated for each image during graph construction. This calculation of a dynamic r_A is more flexible and increases the probability that a cell nuclei segment is connected to its nearest neighbors irrespective of their actual distance in the tissue. However, for the computation of r_A, a uniform distribution assumption in the ideal case is not completely indicative of the heterogeneous tumor tissue in the real case. It should be specified that the assumption does not determine actual edge lengths but only puts a threshold on the connectivity between tissue components, and such a linking approach can result in multiple connected components in the cell nuclei ARG representing true spatial arrangements. Nevertheless, it will be interesting to observe the behavior of dynamically and automatically calculated r_A without requirement of empirical determination, and compare the performance of the two edge linking approaches.

On comparing the computational complexities of the two linking rules, fixed r method has lower costs as it does not require r calculation for each image. On the other hand, accuracy of the assumption of r affects the subsequent classification performance, hence, should be carefully determined using experimental evidence, which increases the overhead related to fixed r method.

2) Cell nuclei ARG construction based on vertex information: Four construction methods based on the information in the graph vertices have been explored as follows.

Generic cell nuclei ARG $(gARG)$**:** As the name suggests, $gARG$ is constructed using all the cell nuclei segments comprising the image as its vertices, irrespective of their individual identities.

Nuclei-specific cell nuclei ARG $(nsARG)$**:** It is constructed by considering all the cell nuclei of the same class. The class for each cell nuclei segment is automatically computed using the cell nuclei classification step of image pre-analysis. Each $nsARG$ represents the spatial arrangements of one of the four cell nuclei classes, namely, *Epithelial Cells*, *Leukocytes*, *Fibrocytes* and *Conglomerates*. Other classes are not considered due to insignificant occurrence and (or) impact. Thus, a maximum of four $nsARG$s are generated for each region of interest. Their vertex attributes do not include morphological and contour intensity based measures because these are utilized during cell nuclei classification. Hence, the construction emphasizes purely on the neighborhood interactions among cell nuclei of the same type in the tissue.

Nuclei-composite cell nuclei ARG $(ncARG)$**:** In this construction, class for each cell nuclei segment is automatically estimated as one of the classes [10] using cell nuclei classification, however, the graph is constructed by considering all the cell nuclei with their identities leading to a single $ncARG$ per image. Its vertex attributes do not include some cell nuclei features due to the reason described for $nsARG$, but an additional vertex attribute denoting the class of each vertex is introduced. The difference of $ncARG$ from $nsARG$ and $gARG$ constructions is the inclusion of all cell nuclei in the same graph with their identities, emphasizing their inter-class relationships in the tissue neighborhood.

Nuclei-composite cell nuclei ARG with additional vertex attributes $(ncARG_{v+})$**:** It is constructed similar to $ncARG$, however, it includes morphological and contour intensity based vertex attributes in addition to the class information of each vertex. This can be seen as repetitive use of vertex attributes, first during cell nuclei classification and then graph construction, though knowledge of existing graphs may be enriched by such reuse.

Among the four construction methods, $gARG$ has the lowest space and time requirements due to its simplistic and straightforward implementation. $ncARG$ and $ncARG_{v+}$ have intermediate requirements due to additional cell nuclei classification. $nsARG$ is the most computationally intensive due to multiple graphs constructed per image in addition to the cell nuclei classification, and requires additional space when the corresponding graphs need to be explicitly saved.

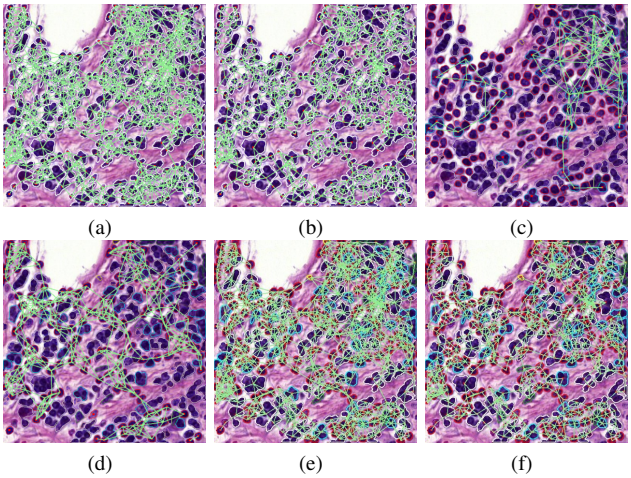

Figure 3: Cell nuclei ARG variants for an example image (a) $gARG[r_F]$ (b) $gARG[r_A]$ (c) $nsARG[r_F]$ {*Epithelial Cells*} (d) $nsARG[r_A]$ {*Leukocytes*} (e) $ncARG[r_F]$ (f) $ncARG[r_A]$ (corresponding $ncARG$ and $ncARG_{v+}$ will have same appearance but different vertex information).

Based on combinations of the two design variables, eight cell nuclei ARG variants are developed, representing a range of the contained knowledge of corresponding tissue regions. $gARG[r_F]$ is the most elementary and intuitive type and

was also initially explored in [2]. More proposed variants are $gARG[r_A]$, $nsARG[r_F]$, $nsARG[r_A]$, $ncARG[r_F]$, $ncARG[r_A]$, $ncARG_{v+}[r_F]$ and $ncARG_{v+}[r_A]$. The graph variants for an example image are depicted in Figure 3.

E. Global Graph Features

These are the moment-based and size-based features computed for each cell nuclei ARG [2]. Moment-based features of the vertex and edge attributes are calculated as their mean, variance, skewness and kurtosis, and minimum and maximum values are also included. Size-based features include number of vertices, number of edges, number of connected components, cyclomatic number, graph density, graph irregularity and number of triangles. A feature vector of 332 global graph features is extracted for each image tile using the $gARG$ construction [2]. For the $nsARG$ construction, a maximum of four graphs and 188 features per graph are generated, yielding a total of 752 global graph features for each image. The $ncARG$ and $ncARG_{v+}$ constructions consist of seven additional global graph features related to vertex identities as the total instances of each type of cell nuclei, hence, a set of 195 and 339 global graph features are extracted from the corresponding graphs respectively.

F. Random Forests Learning and Classification

Random forests is an ensemble learning algorithm involving the training of multiple decision trees and the classification result is the mode of predictions of constituent trees [15]. Random forest has been selected for this work because of high prediction accuracy among traditional machine learning methods, also showing success in digital pathology problems [16], [17].

The learning phase of random forests for our classification task requires prior selection of two experimental parameters, namely, number of decision trees N_t and number of features m for best split. These are estimated by measuring the out-of-bag error for each observation via bootstrap aggregation [18], [19]. A range of values of N_t and m are considered as $N_t \in \{1, 2, ...1500\}$ and $m \in \{log_2 M, \sqrt{M}, M\}$, where M is the total number of extracted features, and suitable values are selected at which the out-of-bag error becomes steady and low. Using random forests, a *hierarchical* classification strategy is explored. It is a two-stage binary classification, where the first stage discriminates between non-tumor and tumors, followed by HER2+ tumor or HER2- tumor prediction in the second stage.

III. Results and Discussion

A total of 795 image tiles have been generated from labeled WSI data, with nearly equal distribution in each of the three malignancy types. Quantitative evaluation is performed using multiple rounds of two cross validation methods, namely, *k-fold stratified shuffled split* and *leave-a-patient-out* [2]. A comparative evaluation scheme is considered for experimental analysis, including state-of-the-art feature extraction methods in digital histopathology and the proposed eight cell nuclei ARG variants. State-of-the-art includes low-level (pixel-based) features using a combination of texture and color selected from GLCM statistics [20], Gabor filter-banks [21], LBP histograms [22], Varma-Zisserman textons [23] and RGB histograms after correlation analysis [2]. It also includes object-level features using the morphological and contour intensity information of cell nuclei [24], [10] without any neighborhood properties or global architecture. High-level state-of-the-art methods include global features from Voronoi diagrams and Delaunay triangulation [1] of the tissue images. Finally, a hybrid set of low-level and high-level features of the most favorable cell nuclei ARG variant are also quantitatively analyzed to represent comprehensive knowledge in the gastric cancer WSI. The overall classification performance for the twelve image description methods in comparative evaluation is summarized in Figure 4, showing the averaged per-class and balanced classification accuracy (BCA) [25] and respective standard deviations.

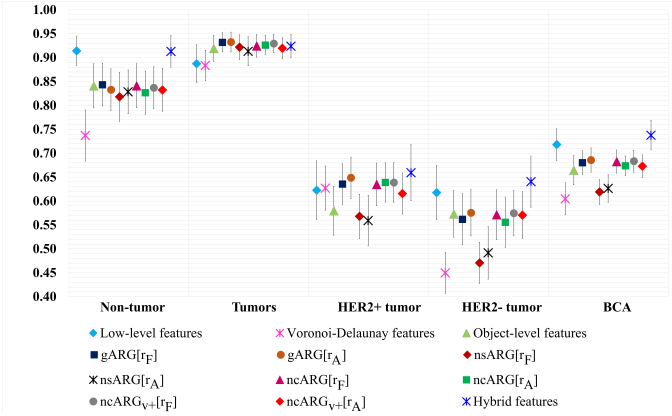

Figure 4: Experimental results: per-class and balanced classification accuracy of the comparatively analyzed methods.

On comparing the class-wise performance of the random forests hierarchical classification, it is evident that in the first stage, higher-level tumors and non-tumor classes attain superior prediction rates due to distinct visual appearances, however, in the second stage, the two tumor subclasses, namely, HER2+ tumor and HER2- tumor are more difficult to discern in the H&E stain. HER2+ tumor has intermediate recognition rate and discrimination from the other tumor type. The most complex class is HER2- tumor with highest prediction error and confusion with HER2+ tumor. This is because HER2- tumor has less distinct visual properties in the H&E stain due to a lower malignancy level and also showed fainter IHC response in the HER2 WSI.

The relative performance between the investigated state-of-the-art methods and proposed cell nuclei ARG variants is elaborated as follows. In the first stage of hierarchical classification, low-level features are superior to proposed graph-based methods for the non-tumor class, but a better

description of tumors is found to be achieved by the cell nuclei ARG variants, and in the second stage, a few graph variants outperform the pixel-based features for HER2+ tumor. Moreover, high-level state-of-the-art features using Voronoi diagrams and Delaunay triangulation do not perform satisfactorily in the first stage and only show good detection for HER2+ tumor in the second stage but at the cost of HER2- tumor. Similarly, object-based features are not as effective as the information extracted from the designed graphs, seen mainly in both the tumor classes of first stage and HER2+ tumor in second stage, with an overall lower detection rate. This observation emphasizes the significance of neighborhood properties, spatial arrangements and architectural information in addition to individual tissue components for knowledge description in histopathological images.

For comparison between cell nuclei ARG variants, classification performance with respect to the two design variables is analyzed. On investigating the linking rules, the two counterparts show comparable performance with small overall variations, *i.e.* increase in $gARG$ and $nsARG$ but decline in $ncARG$ and $ncARG_{v+}$ with the adaptive r approach. However, fixed r bears the overhead of empirical selection depending on nature of datasets, so adaptive r can be more conveniently computed to generate descriptive cell nuclei ARGs without significant deviation in performance. Among the four construction methods, $ncARG$ is most promising with close similarity to $gARG$, that outperform $ncARG_{v+}$ and $nsARG$ methods in order. Clearly, $nsARG$ is unsuitable with consistently lower detection rates specifically in the second stage of hierarchical classification. This is mainly due to the inclusion of selective interactions of specific cell types that may not be as meaningful as their global interactions in the tissue. Also, the omitted vertex attributes deplete the graph of useful information about individual cells and affects the decision-making process. Furthermore, $ncARG_{v+}$ does not depict any significant improvement over $ncARG$ by reuse of vertex attributes with cell nuclei identities. On comparing $gARG$ and $ncARG$, it can be argued that these graphs are two representations of the same information, with former containing 'raw' moment-based features of vertex attributes, and the latter with 'processed' features after these attributes facilitate cell nuclei classification. However, $ncARG$ is more adequate because $gARG$ generates a larger number (nearly 1.7 times) of global graph features compared to $ncARG$, so the final classifier decision is more prone to error due to higher dimensionality [26]. In contrast, if vertex attributes are first applied to predict cell types, and measures reflecting tissue composition (number of each cell type) are then added to global graph features, a cleaner feature vector is obtained. The $ncARG$ method has further potential of enhancement with improvements in cell nuclei segmentation and classification, however, demands higher computational requirements than $gARG$ due to cell nuclei classification.

Lastly, the hybrid approach for combination of knowledge using low-level state-of-the-art and high-level handcrafted features exhibits the highest prediction performance (average BCA=73.78%) in both classification stages, which suggests that the fusion of complimentary pixel-based and architectural information can lead to further enhancement in the tissue image descriptions, also observed in [2]. This is followed by the low-level features (average BCA=71.83%), and high-level handcrafted graph-based features using $gARG[r_A]$ (average BCA=68.58%), $ncARG_{v+}[r_F]$(average BCA=68.36%) and $ncARG[r_F]$ (average BCA=68.26%) variants of the cell nuclei ARG. Hence, the proposed novel cell nuclei ARG graph-based method compares favorably to most state-of-the-art feature extraction approaches leading to effective description and classification in H&E gastric cancer WSI based on HER2 IHC.

IV. Conclusion

In this paper, a set of solutions using high-level graph-based methods is proposed for modeling and quantifying meaningful information in H&E stained gastric cancer WSI. The cell nuclei ARG method is thoroughly explored, where eight graph variants are implemented and comparatively analyzed, also with widely known state-of-the-art feature extraction approaches. The experimental results using hierarchical random forests classification depict that some of the proposed graphs are superior than other variants, and also comparable to state-of-the-art methods. Specifically, the $ncARG$ construction with fixed or adaptive r has desirable properties and outcome in gastric cancer classification based on HER2 IHC. Furthermore, it can be established that the information extracted from cell nuclei ARG variants including individual cells, neighborhood relationships and global tissue architecture can enhance the knowledge obtained purely at the object-level, and can further enrich the pixel-based texture and color measures of tissue images. This work can contribute towards assisting pathologists in computer-aided diagnosis tasks, and reducing manual efforts and observer variability in digital histopathology.

An advantage of the discussed handcrafted descriptors is their enhanced scope of interpretation in histopathological images with special characteristics such as complex appearances and high resolutions. However, certain errors may be introduced during image pre-analysis in cell nuclei segmentation and classification prior to the graph construction and affect the classifier decision. In contrast, deep learning methods process raw images directly and do not necessary require image pre-analysis. We have performed a comparative study between deep convolutional neural networks and low-level features with traditional machine learning [27] for the described cancer classification problem in H&E stained gastric cancer WSI. Similarly, a comparative study of the proposed high-level graph-based handcrafted methods and deep learning will be an exciting research prospect. Extension of the current gastric carcinoma reference WSI dataset

with more number of patients will increase the robustness of the proposed system. Exploring the repeatability of our methods using open source benchmark datasets will also be an interesting future direction.

REFERENCES

[1] H. Sharma, N. Zerbe, S. Lohmann, K. Kayser, O. Hellwich, and P. Hufnagl, "A review of graph-based methods for image analysis in digital histopathology," *Diagnostic Pathology*, vol. 1, no. 1, 2015.

[2] H. Sharma, N. Zerbe, D. Heim, S. Wienert, S. Lohmann, O. Hellwich, and P. Hufnagl, "Cell nuclei attributed relational graphs for efficient representation and classification of gastric cancer in digital histopathology," in *SPIE Medical Imaging*. International Society for Optics and Photonics, 2016, pp. 97 910X–97 910X.

[3] M. N. Gurcan, L. E. Boucheron, A. Can, A. Madabhushi, N. M. Rajpoot, and B. Yener, "Histopathological image analysis: A review," *Biomedical Engineering, IEEE Reviews in*, vol. 2, pp. 147–171, 2009.

[4] C. Gunduz, B. Yener, and S. Gultekin, "The cell graphs of cancer." in *ISMB/ECCB (Supplement of Bioinformatics)*, 2004, pp. 145–151.

[5] C. Bilgin, C. Demir, C. Nagi, and B. Yener, "Cell-graph mining for breast tissue modeling and classification," in *Engineering in Medicine and Biology Society, 2007. EMBS 2007. 29th Annual International Conference of the IEEE*. IEEE, 2007, pp. 5311–5314.

[6] C. C. Bilgin, P. Bullough, G. E. Plopper, and B. Yener, "ECM-aware cell-graph mining for bone tissue modeling and classification," *Data mining and knowledge discovery*, vol. 20, no. 3, pp. 416–438, 2010.

[7] H. Sharma, A. Alekseychuk, P. Leskovsky, O. Hellwich, R. Anand, N. Zerbe, and P. Hufnagl, "Determining similarity in histological images using graph-theoretic description and matching methods for content-based image retrieval in medical diagnostics," *Diagnostic pathology*, vol. 7, no. 1, p. 134, 2012.

[8] S. Arslan, T. Ersahin, R. Cetin-Atalay, and C. Gunduz-Demir, "Attributed relational graphs for cell nucleus segmentation in fluorescence microscopy images," *IEEE Transactions on Medical Imaging*, vol. 32, no. 6, pp. 1121–1131, June 2013.

[9] K. Kayser, K. Sandau, G. Böhm, K. D. Kunze, and J. Paul, "Analysis of soft tissue tumors by an attributed minimum spanning tree." *Analytical and quantitative cytology and histology/the International Academy of Cytology [and] American Society of Cytology*, vol. 13, no. 5, pp. 329–334, 1991.

[10] H. Sharma, N. Zerbe, D. Heim, S. Wienert, H.-M. Behrens, O. Hellwich, and P. Hufnagl, "A multi-resolution approach for combining visual information using nuclei segmentation and classification in histopathological images," in *Proceedings of the 10th International Conference on Computer Vision Theory and Applications (VISIGRAPP 2015)*, 2015, pp. 37–46.

[11] H. Behrens, V. Warneke, C. Böger, N. Garbrecht, E. Jüttner, W. Klapper, M. Mathiak, I. Oschlies, U. Rudolph, C. Stuhlmann-Laeisz *et al.*, "Reproducibility of Her2/neu scoring in gastric cancer and assessment of the 10% cut-off rule," *Cancer medicine*, vol. 4, no. 2, pp. 235–244, 2015.

[12] J. Bancroft and M. Gamble, *Theory and practice of histological techniques*. Elsevier Health Sciences, 2008.

[13] V. Warneke, H. Behrens, C. Böger, T. Becker, F. Lordick, M. Ebert, and C. Röcken, "Her2/neu testing in gastric cancer: evaluating the risk of sampling errors," *Annals of Oncology*, vol. 24, no. 3, pp. 725–733, 2013.

[14] S. Wienert, D. Heim, K. Saeger, A. Stenzinger, M. Beil, P. Hufnagl, M. Dietel, C. Denkert, and F. Klauschen, "Detection and Segmentation of Cell Nuclei in Virtual Microscopy Images: A Minimum-Model Approach," *Scientific Reports*, vol. 2, 2012.

[15] L. Breiman, "Random forests," *Machine learning*, vol. 45, no. 1, pp. 5–32, 2001.

[16] J. Wang, J. D. MacKenzie, R. Ramachandran, and D. Z. Chen, "Identifying neutrophils in H&E staining histology tissue images," in *Medical Image Computing and Computer-Assisted Intervention (MICCAI 2014)*. Springer, 2014, pp. 73–80.

[17] M. D. DiFranco, G. OHurley, E. W. Kay, R. W. G. Watson, and P. Cunningham, "Ensemble based system for whole-slide prostate cancer probability mapping using color texture features," *Computerized medical imaging and graphics*, vol. 35, no. 7, pp. 629–645, 2011.

[18] J. Friedman, T. Hastie, and R. Tibshirani, *The elements of statistical learning*. Springer series in statistics Springer, Berlin, 2001, vol. 1.

[19] F. Pedregosa, G. Varoquaux, A. Gramfort, V. Michel, B. Thirion, O. Grisel, M. Blondel, P. Prettenhofer, R. Weiss, V. Dubourg, J. Vanderplas, A. Passos, D. Cournapeau, M. Brucher, M. Perrot, and E. Duchesnay, "Scikit-learn: Machine learning in Python," *Journal of Machine Learning Research*, vol. 12, pp. 2825–2830, 2011.

[20] R. M. Haralick, K. S. Shanmugam, and I. Dinstein, "Textural features for image classification," *IEEE Transactions on Systems, Man and Cybernetics*, vol. 3, no. 6, pp. 610–621, 1973.

[21] S. Marčelja, "Mathematical description of the responses of simple cortical cells," *JOSA*, vol. 70, no. 11, pp. 1297–1300, 1980.

[22] T. Ojala, M. Pietikäinen, and D. Harwood, "A comparative study of texture measures with classification based on featured distributions," *Pattern recognition*, vol. 29, no. 1, pp. 51–59, 1996.

[23] M. Varma and A. Zisserman, "Classifying images of materials: Achieving viewpoint and illumination independence," in *Computer VisionECCV 2002*. Springer, 2002, pp. 255–271.

[24] P. Hufnagl, A. Schlosser, and K. Voss, "Merkmale der Form, Gröβe und Lage digitaler objekte." *Bild und Ton.*, vol. 37, pp. 293–298, 1984.

[25] K. Brodersen, C. Ong, K. Stephan, and J. Buhmann, "The balanced accuracy and its posterior distribution," in *Pattern recognition (ICPR), 2010 20th international conference on*. IEEE, 2010, pp. 3121–3124.

[26] G. Hughes, "On the mean accuracy of statistical pattern recognizers," *IEEE Transactions on Information Theory*, vol. 14, no. 1, pp. 55–63, Jan 1968.

[27] H. Sharma, N. Zerbe, I. Klempert, O. Hellwich, and P. Hufnagl, "Deep convolutional neural networks for automatic classification of gastric carcinoma using whole slide images in digital histopathology," *In Press: Computerized Medical Imaging and Graphics*, 2017.